Pergamon

Bioorganic & Medicinal Chemistry 10 (2002) 3529–3544

BIOORGANIC & MEDICINAL CHEMISTRY

Tetrahydroisoquinoline-3-carboxylate Based Matrix-Metalloproteinase Inhibitors: Design, Synthesis and Structure–Activity Relationship

Hans Matter,* Manfred Schudok*, Wilfried Schwab, Werner Thorwart, Denis Barbier, Günter Billen, Burkhard Haase, Bernhard Neises, Klaus-Ulrich Weithmann and Theo Wollmann

Aventis Pharma Deutschland GmbH, D-65926 Frankfurt am Main, Germany

Received 21 February 2002; accepted 7 June 2002

Abstract—The design, synthesis and structure–activity relationship (SAR) of a series of nonpeptidic 2-arylsulfonyl-1,2,3,4-tetrahydro-isoquinoline-3-carboxylates and-hydroxamates as inhibitors of the matrix metalloproteinase human neutrophil collagenase (MMP-8) is described here. Based on available X-ray structures of MMP-8/inhibitor complexes, our structure-based design strategy was directed to complement major protein-ligand interaction regions mainly in the S1′ hydrophobic specificity pocket close to the catalytic zinc ion. Here, the rigid 1,2,3,4-tetrahydroisoquinoline scaffold (Tic) provides ideal geometry to combine hydroxamates and carboxylates as typical zinc complexing functionalities, with a broad variety of S1′ directed mono- and biaryl substituents consisting of aromatic rings perfectly accommodated within this more hydrophobic region of the MMP-8 inhibitor binding site. The effect of different S1′ directed substituents, zinc-complexing groups, chirality and variations of the tetrahydroisoquinoline ring-system is investigated by systematic studies. X-ray structure analyses in combination with 3D-QSAR studies provided an additional understanding of key determinants for MMP-8 affinity in this series. The hypothetical binding mode for a typical molecule as basis for our inhibitor design was found in good agreement with a 1.7 Å X-ray structure of this candidate in complex with the catalytic domain of human MMP-8. After analysis of all systematic variations, 3D-QSAR and X-ray structure analysis, novel S1′ directed substituents were designed and synthesized and biologically evaluated. This finally results in inhibitors, which do not only show high biological affinity for MMP-8, but also exhibit good oral bioavailability in several animal species.

Introduction

Matrix metalloproteinases (MMPs) are a family of zinc endopeptidases which are capable of degrading the extracellular matrix of connective tissues.[1] They are broadly implicated in a number of degenerative diseases in which there is a slow matrix degradation rate, including cartilage loss in osteoarthritis[2] and rheumatoid arthritis,[3] bone matrix degradation in osteoporosis or remodeling in Alzheimer disease.[4] All the MMPs possess three discrete domains: a propeptide (~80 AS) cleaved during activation, a catalytic domain (~180 AS) including a conserved HEXXHXXGXXH zinc binding motif, and a hemopexin-like domain (~250 AS), presumably responsible for substrate recognition.[5] Stromelysin (MMP-3), as well as particularly the intestinal fibroblast collagenase (MMP-1) and the neutrophil collagenase (MMP-8) are responsible for the cleavage of type I-, II- and III-collagen, and therefore regarded as key enzymes in the pathology of matrix degradation.

Thus, selective inhibitors targeted against these collagenases have become attractive for rational drug design. At an early stage, peptidic inhibitors were designed based on the knowledge of the natural substrate located at the catalytic site of the enzyme. Combined with a thiol-, phosphonic-, carboxylic- or hydroxamic-acid group as zinc chelating function, they achieve in vitro inhibitory activity in the nanomolar range.[6] However, those substrate-orientated inhibitors show low oral bioavailibility, which might be related to their peptidic nature. Hence, our design was directed towards conformationally restricted nonpeptidic inhibitors combining high affinity, selectivity, and improved pharmacokinetic properties.

*Corresponding authors. Tel.: +49-69-305-84329; fax: +49-69-331399; e-mail: hans.matter@aventis.com (H. Matter); e-mail: manfred.schudok@aventis.com (M. Schudok).

0968-0896/02/$ - see front matter © 2002 Elsevier Science Ltd. All rights reserved.
PII: S0968-0896(02)00215-8

In this study the design, synthesis, and structure–activity relationship (SAR) for a novel inhibitor series is presented. Stimulated by X-ray structures of human MMP-8 with low molecular weight ligands,[7–11] the rigid 1,2,3,4-tetrahydroisoquinoline scaffold (Tic) was chosen as central scaffold. Consequently, a series of 2-arylsulfonyl-1,2,3,4-tetrahydro-isoquinoline-3-carboxylates **1a**, hydroxamates **1b** and their corresponding isoquinolines analogues targeting MMP-8 was designed, synthesized and biologically evaluated (Scheme 1). The systematic variation of different mono- and biaryl ring systems directed towards the hydrophobic MMP S1′ specificity pocket,[12] zinc-complexing groups, chiralities at the Tic-C3 carbon and variations at the aromatic moiety of the tetrahydroisoquinoline scaffold is described in this publication and led us to establish a detailed SAR prior to a second design cycle in search for more potent analogues in this series (cf. Fig. 1).

In order to unravel the underlying SAR for this system, all molecules were docked into the binding site of MMP-8, as defined using 3D structures of the MMP-8

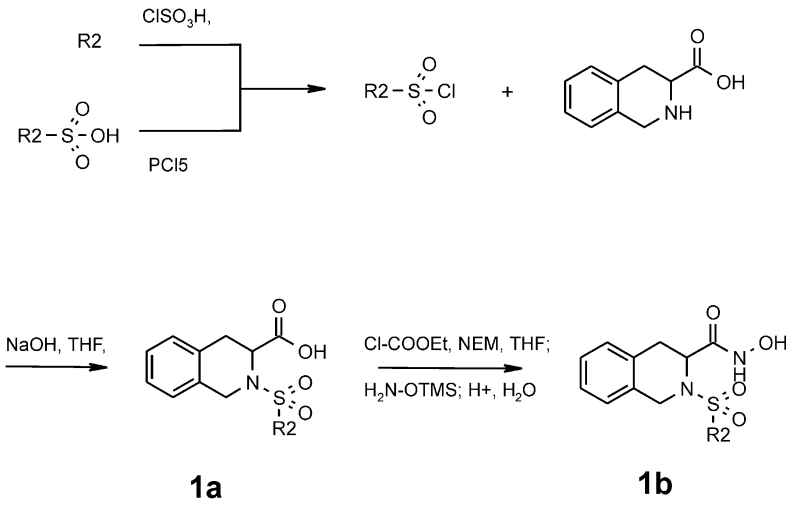

Scheme 1. Synthesis of 2-orylsulfonyl-1,2,3,4-tetrahydroisoquinoline-3-carboxylates and -hydroxamates.

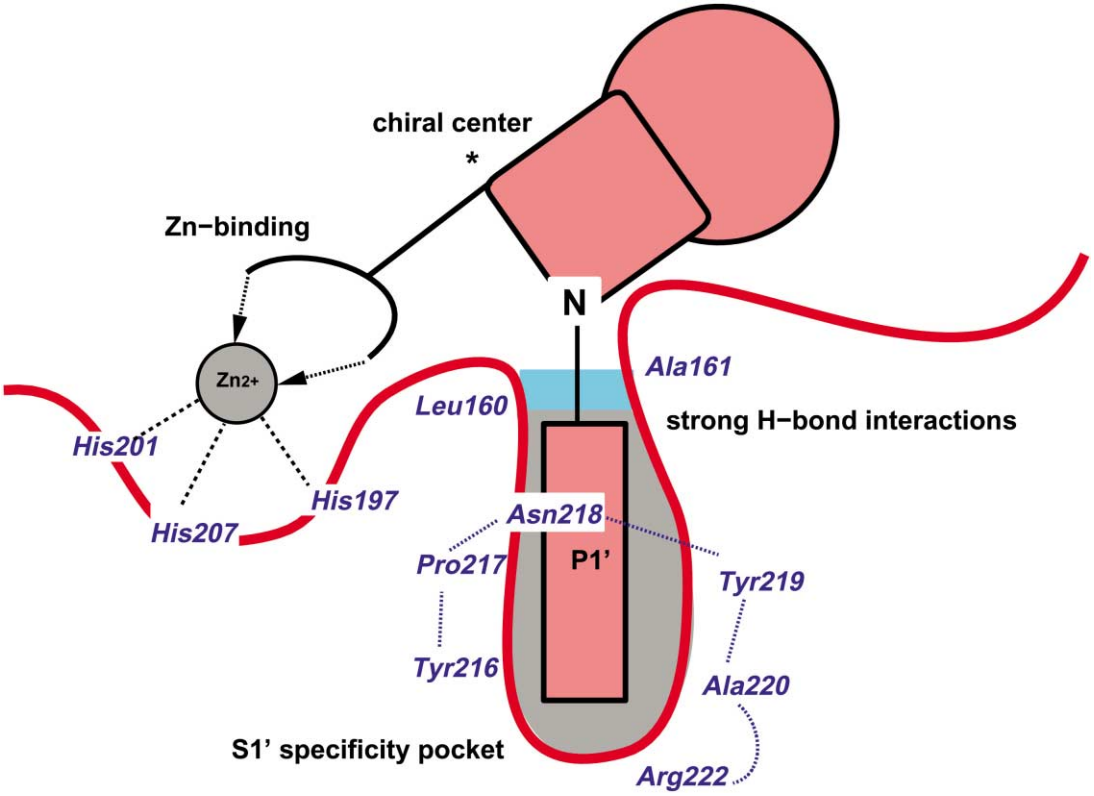

Figure 1. Schematic view to the MMP-8 binding site with key residues indicated. The bicyclic 1,2,3,4-tetrahydroisoquinoline scaffold provides ideal geometry to link S1′ directed hydrophobic substituents with zinc complexing groups. Hydrogen bond acceptors are favourable at the S1′ entrance, while the aromatic 1,2,3,4-tetrahydroisoquinoline ring is situated close to a hydrophobic region.

catalytic domain with different peptides.[9,13] This led to a binding hypothesis for all compounds from this series by superimposing them onto the template and minimizing them within the MMP-8 binding site. The resulting superpositions produced consistent 3D-QSAR models using CoMFA and related methods,[14–18] allowing to rationalize ligand–enzyme interactions by deriving a significant and predictive relationship between molecular property fields and biological activities. Details of the 3D-QSAR-studies have been published elsewhere,[19,20] while the qualitative structure–activity relationship reported in this contribution in combination with those results plus X-ray data[19] formed the basis for further structure-based design of potent, bioavailable candidates in a second iterative design cycle. This finally led to the discovery of potent and bioavailable inhibitors targeted against MMP-8 presented here.

Structure-Based Design of MMP-8 Inhibitors

All inhibitors were designed based on active site geometries from public domain MMP-8 X-ray stuctures (cf. Figs 2 and 3). The specificity of collagenases to cleave at medium-sized hydrophobic residues is tightly connected to size, electrostatic and hydrophobic properties of the S1′ specificity pocket close to the catalytic Zn^{2+} ion. This pocket's wall is formed by Pro217-Asn218-Tyr219,[21] while its entrance is built by Gly158 to Ala161 and the aromatic sidechain from Tyr219, opening into a hydrophobic interior. The S1′ bottom is occupied by the polar Arg222, its side chain being flexible, adopting different conformations in different X-ray structures. The terminal guanidine is hydrogen bonded to the carbonyl groups of Pro211, Gly212 (via solvent) and Ala213. In most X-ray structures the S1′ pocket is filled with two or three solvent molecules interacting with the Arg222 guanidine and other polar backbone atoms.

Several hydrophobic and hydrogen-bonding regions in the MMP-8 binding site (Figs 2 and 3) were identified using GRID with appropriate probe atoms[22] and by visual inspection of protein-ligand complexes. It was found that a rigid 1,2,3,4-tetrahydroisoquinoline provides ideal geometry to connect zinc binding groups with S1′ directed substituents. Its heterocyclic ring is situated at the entrance to the active site between Ile159 and His207, with appropriate bond vectors at C3 and N2 pointing towards the catalytic zinc and the S1′ pocket, respectively. The hydrophobic aromatic ring is close to a hydrophobic region identified using GRID (dry probe) at the surface of the cavity (Fig. 2B and C) comprising of the plane of the His207 imidazole ring, and, for example, being occupied by an thiophene in the inhibitor present in the PDB structure *1mmb*.[10] When chirality is inverted at C3, the biological activity decreases, as this favourable hydrophobic interaction is not longer possible.[19]

Hydrogen bonds to ligands involving the amide protons of Leu160 and Ala161 at the S1′ entrance are to be found in these X-ray structures.[7–11] In our design, the sulfonyl-oxygen atoms of the sulfonamide attached to the rigid tetrahydroisoquinoline scaffold via nitrogen N2 are added to complementary interactions at the S1′ entrance. Furthermore this linkage allows for many synthetic variations to explore S1′ pocket binding requirements (Fig. 3C) Hydroxamates and carboxylates were chosen as zinc complexing groups. Although carboxylates do not exhibit optimal zinc binding properties, it has been demonstrated earlier that they relate to higher bioavailability.[23,24] Thus is was considered by us[19,20] and others[23–26] to compensate any expected loss in binding affinity by adding substituents with optimal complementarity to the S1′ pocket.

The aromatic sidechains of Tyr219 and His197 at opposite sides of the S1′ wall here suggest that favourable contribution to binding energy could result from protein–ligand aryl–aryl interactions within the S1′ pocket.[27] Thus, aromatic residues (monoaryl, biaryl and biarylether substituents) were incorporated, which, at the same time, are replacing crystallographically conserved water molecules.

The postulated binding mode for inhibitor design was later validated using an 1.7 Å X-ray structure analysis ([xix]) of the MMP-8/**62** complex with a biphenyl substituent directed towards S1′. The experimental binding mode of compound **62** is shown in Figure 2D (green carbons) compared to 10 best docking modes (white carbons) obtained using the program FlexiDock.[28] Both oxygens of the 3-carboxyl group are in coordination with the catalytic zinc, one sulfonamide oxygen is exposed to the solvent, while the other is hydrogen bonded to Leu160-NH and Ala161-NH. The biphenyl inside S1′ is stacked on top of the His197 imidazole, and the loop from Leu214 to Ala220 wraps around the inhibitor. As obvious the experimental binding mode is similar to our template for design. The 3D-QSAR analyses are discussed elsewhere,[19,20] their results in combination with X-ray structure investigations then led to a successful second design cycle (see below).

Chemistry

The target series[29] of 2-arylsulfonyl-1,2,3,4-tetrahydroisoquinoline-3-carboxylates **1a** and -hydroxamates **1b** were synthesized according to Scheme 1. Biaryl-substituents were selected according to the design strategy and taking synthetic availability as additional constraints into account. This reaction sequence was applied for the majoritiy of candidate molecules. Most syntheses proceeded either under standard or slightly modified conditions, as reported below.

Sulfonyl chlorides were commercially available or prepared by treatment of the corresponding sulfonic acids or their salts with chlorination agents (PCl_5, $POCl_3$ or $SOCl_2$) under standard procedures. Alternatively, an aromatic ring system was sulfochorinated in para-position using chlorosulfonic acid. The synthesis of the chlorobiphenylethyl-sulfonylchloride building block as an example for an alkyl sulfonamide resulting from the second design cycle and is outlined in Scheme 2. The

formation of tetrahydroisoquinoline-sulfonamides **1a** was done using standard Schotten–Baumann conditions. Preferred solvents were THF or THF/DMF-mixtures, NaOH or organic bases like DIPEA were applied. The conversion to the corresponding hydroxamates **1b** was achieved by activation of the acids as mixed anhydride (isobutyl or ethyl chloroformate and NMM or NEM) or acid chloride (oxalyl chloride) and reaction

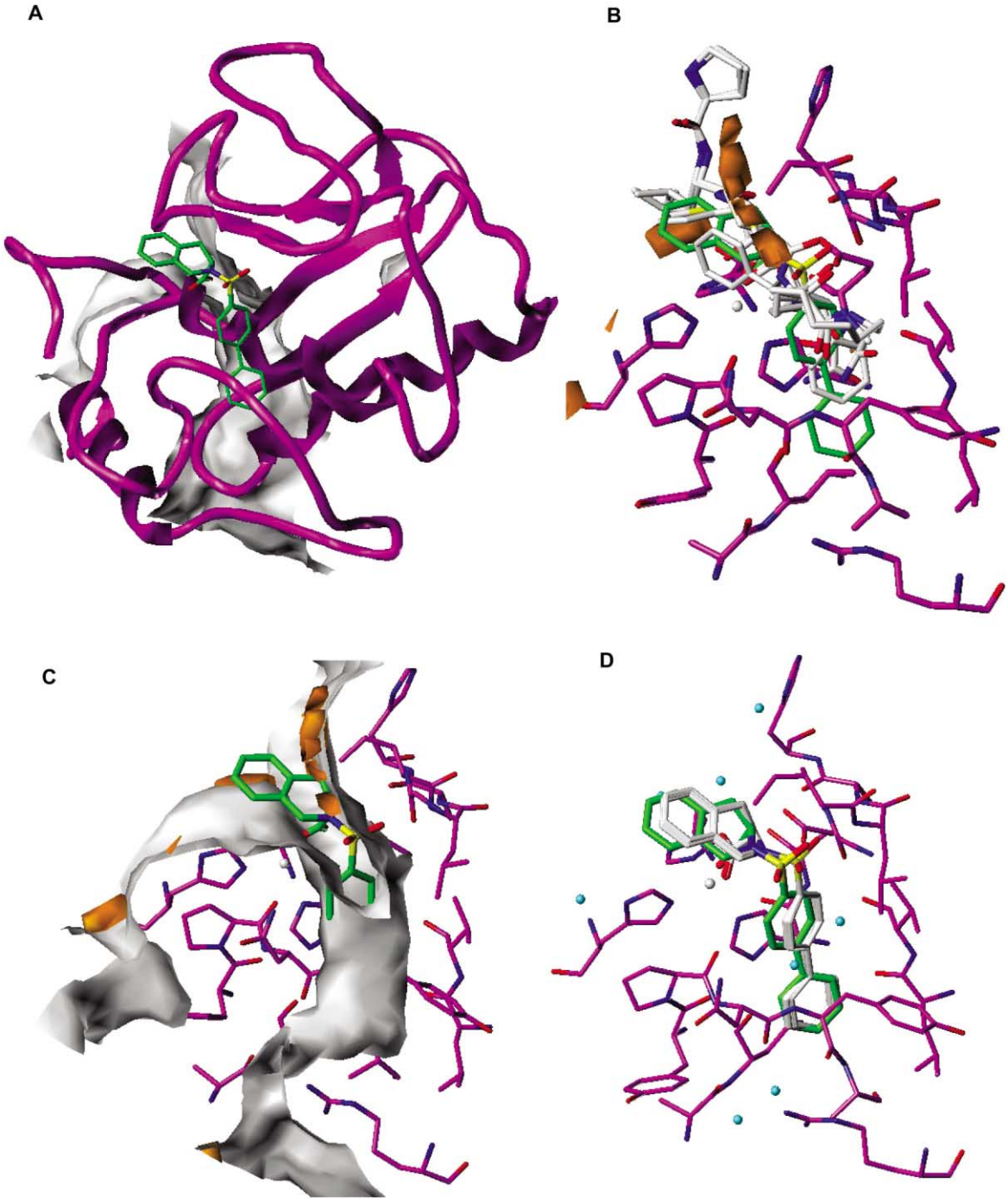

Figure 2. (A) Human neutrophil collagenase (MMP-8) fold from a 1.7 Å X-ray structure of the MMP-8/**62** complex,[19] indicated by a magenta ribbon-tube encoding secondary structure elements, while compound **62** is displayed with green carbons. The MMP-8 inhibitor binding site is highlighted by a GRID[22] interaction energy contour map based on a methyl probe, drawn at +1 kcal/mol. Depth cueing is used to allow for a view into S1′, where the biphenyl substituent is located. Similar models were obtained for public domain inhibitor complexes, serving as basis for our design. (B) Detailed MMP-8 binding site containing compound **62** with green carbons in comparison to public domain inhibitors from PDB files *1jan, 1jao, 1jap, 1jaq, 1mnc, 1kbc, 1mmb*,[13] shown with grey carbons. Magenta carbons indicate selected protein residues from the above X-ray structure. Grey spheres indicate structurally conserved zinc ions. The MMP-8 binding site is highlighted by a GRID interaction energy contour (+1 kcal/mol) using a methyl probe, while hydrophobic regions are indicated by orange contours at −0.3 kcal/mol. (C) Detailed MMP-8 binding site containing compound **62** with green carbons. Regions with favourable hydrophobic interactions are indicated with orange contours at −0.3 kcal/mol from GRID interaction energies using a *hydrophobic* (*DRY*) probe. (D) 1.7 Å X-ray structure[19] of the MMP-8/**62** complex (green carbons) compared to 10 best docking modes using FlexiDock (white carbons) after manual placement of a template in the MMP-8 cavity. Similar docking modes were used as basis for inhibitor design.

with *O*-trimethylsilyl hydroxylamine in THF, followed by treatment with aqueous HCl for deprotection.

Modified 3-Tic (tetrahydroisoquinoline-3-carboxylic acid) derivatives and hetero-analogues were prepared by standard Pictet–Spengler cyclization.[30] Additionally, the 6- or 7-nitro and amino-3-Tic derivates were synthesized by a new method,[31] outlined in Scheme 3.

Starting from commercially available 1,2,3,4-tetrahydroisoquinoline-3-carboxylic acid, the nitration with KNO_3/H_2SO_4 was found to be the best method with respect to regioselectivity and purity. Under strict temperature control, no di-nitration products could be observed, while the excess for the 7-nitration product **30a** is 9-fold. For the synthesis of regiopure compounds, three different ways were used: (a) flash chromatography on silica gel of the carboxylic acid sulfonamides (nitro-stage). However, this was tedious because of the chemical similarity of both isomers. (b) The 2-Boc-6-/7-nitro-Tic could be transformed to the DCHA-salt, which easily could be recrystallized resulting in the pure 7-isomer **30c**. (c) Reduction of the nitro group to the amine. Here, the 6-isomer is slighly better soluble in hot acetonitrile. As expected, the chemistry of the nitro-Tic derivatives was similar to unsubstituted analogues. All compounds in Table 1 were prepared in analogy, compound IDs correspond to ref 19.

Structure–Activity Relationship

The discussion of the structure–activity relationship for 2-arylsulfonyl-1,2,3,4-tetrahydro-isoquinolines (Scheme 1, Table 1) is based on a combined analysis of (a) X-ray structure of the MMP-8/**62** complex,[19,32] (b) 3D-QSAR for 90 analogues[19] and (c) 2-D chemical substitutions. It outlines the rational for designing MMP inhibitors with improved selectivity and pharmacokinetic properties in a second design cyclus.

The tetrahydroisoquinoline ring of **62** is located at the entrance to the active site between Ile159 and His207 with its aromatic part exposed to the solvent. This position was modified during the chemical optimization to improve affinity and physicochemical properties. No significant affinity change was observed upon substitution of the solvent exposed tetrahydroisochinoline moiety, listed as IC_{50} value for MMP-8 in nM. This is obvious from comparison of the compound **21** (4 nM) to **30** with an amino substituent at R3 (2 nM). Furthermore the unsubstituted **49** with an 4-Cl-biphenylsulfonyl group directed towards S1′ is equally active (5 nM) to the corresponding 7-amino derivative **60** at R4 (7 nM).

One of the sulfonamide oxygens is solvent exposed, while the other is involved in hydrogen bonds to Leu160-NH and Ala161-NH and thus essential to maintain biological activity in this series. The biphenyl system attached to this sulfonamide is deeply buried inside the S1′ pocket, stacked on top of the His197 imidazole ring. At the other side, the loop between Leu214 and Ala220 wraps around the inhibitor. This experimental binding mode is similar to that used as template for defining the alignment rule for 3D-QSAR. It was also shown to be consistent with the SAR of this series according to docking studies.

Introducing bulky substituents at the bottom of the MMP-8 S1′ pocket increases biological activity, as

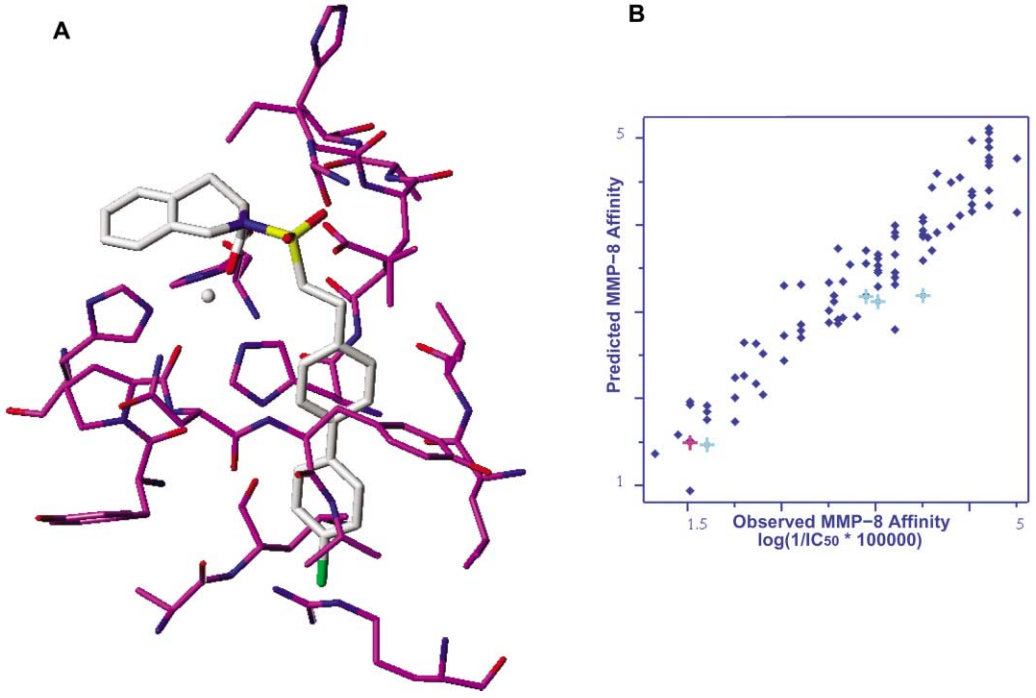

Figure 3. (A) Postulated binding mode of compound **96** within MMP-8 binding site. Only selected amino acid residues are shown. (B) Observed versus predicted MMP-8 affinities for utilized CoMFA model [19] with crossvalidated r^2 value of 0.569 for five components. Compounds used to derive this model are indicated by diamonds, while predictions for five new candidates are indicated by crosses.

exemplified by comparing the following hydroxamates. While the parent compound **9** with phenyl substitution at R2 directed towards the S1′ pocket shows an activity of 20 nM, a 4-methoxy substituent at this phenyl increases activity (**21**, 4 nM). Increasing the size of this substituent by replacing 4-methoxy by 4-phenoxy (**8**, 2 nM) or 4-(4-dimethylamino)-phenoxy (**22**, 2 nM) also improved MMP-8 affinity. Replacing the biarylether moiety by biphenyl substituents attached to the sulfonamide at R1 does not affect biological activity, as exemplified in compounds **23** with 4-biphenyl (2 nM) and **50** with 4-(4-chloro)-biphenyl (3 nM). This corresponds to carboxylates with otherwise unchanged substituents at the central scaffold. However, here the parent compound carrying a 4-methoxy substitution at the S1′ directed phenyl ring shows moderate activity (**29**, 7000 nM) compared to 4-phenoxy or 4-(4-dimethylamino)-phenoxy substitutions (**52**, 9 nM and **63**, 1 nM), respectively. Again the replacement of biarylethers against biphenyls does not significantly affect biological activity, as obvious from compound **62** with 4-biphenyl (10 nM). However, for carboxylates, the effect of steric bulk in the S1′ pocket is more pronounced, as small modifications in that hydrophobic area compensate for the loss of binding affinity in the parent compounds with 4-methoxyphenyl substitution at R2 (**21**, 4 nM as hydroxamate versus **29**, 7000 nM as carboxylate), not optimally accomodating the hydrophobic environment in the lower part of the S1′ pocket in MMP-8. If a second aromatic ring is introduced, differences between zinc binding groups decrease. This observation is in agreement to X-ray structural data and 3D-QSAR, both highlighting a hydrophobic cleft in S1′ formed by the MMP-8 sidechains of Tyr219, Leu193 and Val194. This

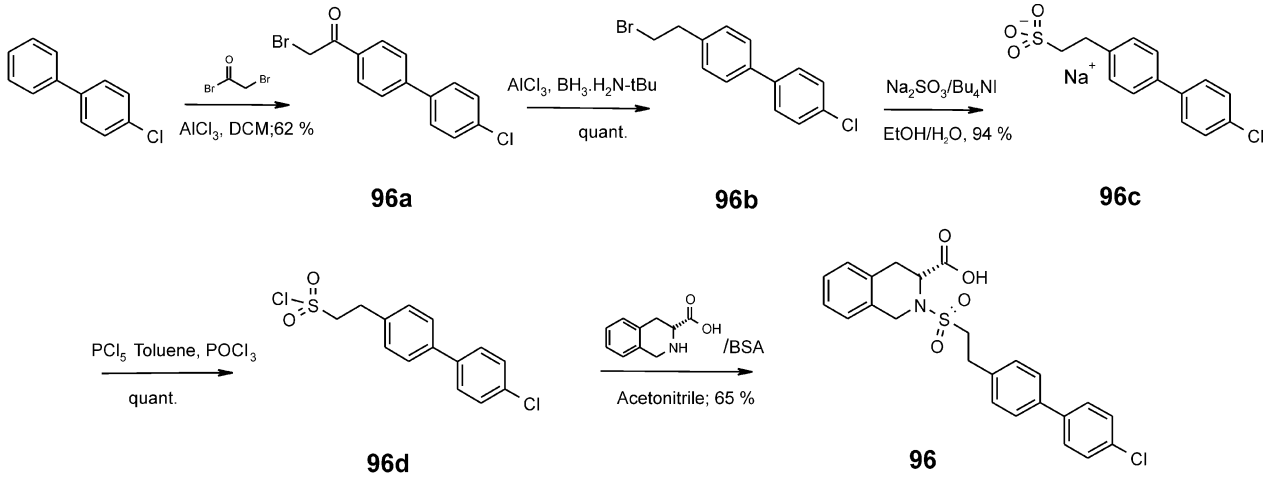

Scheme 2. Synthesis of the chlorobiphenylethyl-sulfonylchloride building block.

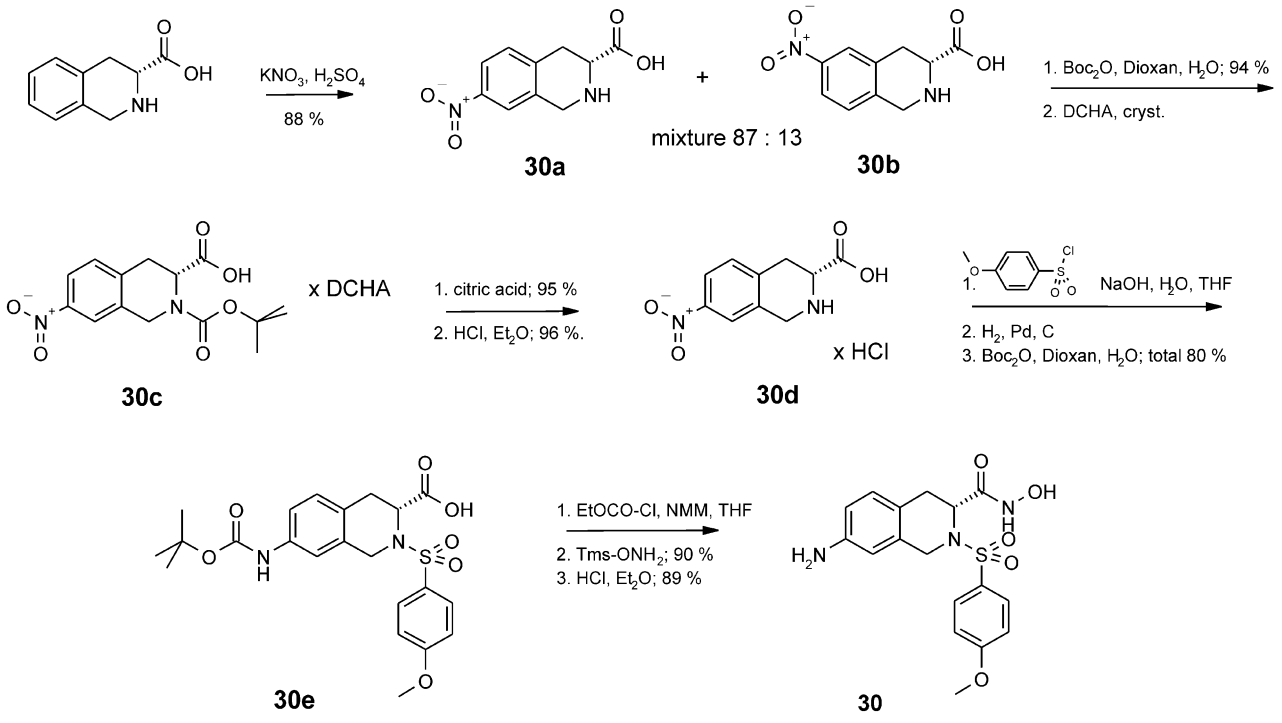

Scheme 3. Synthesis of nitro and amino-3-Tic derivatives.

area is filled with structurally conserved water in several MMP-8–inhibitor complexes, if not replaced by hydrophobic inhibitor parts.

From X-ray structural data and 3D-QSAR, the preferred zinc binding geometry is highlighed, as the optimal distance of two oxygens for zinc coordination is better realized in hydroxamates (2.7 Å) than in carboxylates (2.2 Å). The X-ray structure of **62** showed both carboxylate oxygens interacting with the catalytic zinc ion, while several other X-ray stuctures of different zinc-binding motifs for matrix metalloproteinases support the bidental interaction of these zinc binding motifs. These differences in favourable protein–ligand interactions are exemplified by comparison of compound **29** (carboxylate, 7000 nM) to **21** (hydroxamate, 4 nM) with 4-methoxybenzenesulfonyl substituents, **52** (carboxylate 9 nM) to **8** (hydroxamate, 2 nM) with 4-phenoxybenzenesulfonyl substituents and **49** (carboxylate, 5 nM) to **50** (hydroxamate 3 nM) with 4-chlorobiphenylsulfonyl substituents. Again, it is obvious that reduced binding affinity due to replacement of hydroxamic acids by carboxylic acids can be compensated by S1′-directed substituents with optimal protein–ligand interactions. Such a sterically favourable substitution optimally interacting with the S1′ pocket can lead to carboxylate-based inhibitors with comparable binding affinity to hydroxamates. This has important implications for inhibitor design, as carboxylates are known to exhibit higher oral bioavailability.[23,24] We showed here that inhibitors with weaker zinc binding groups require a compensation by an optimal fit of hydrophobic substituents into the S1′ pocket.[25,26]

The analysis of the 3D-QSAR model at the first biphenylether ring indicates a close proximity of low-affinity ligands to Pro217, His207, Zn^{2+}, His197 or Val194, which correspond to the narrow, polar S1′ entrance. Hence, any substitution at this aromatic ring directly attached to the sulfonamide should reveal a certain shape in order not to undergo unfavourable interactions with those residues flanking this narrow S1′ entrance. At the edge of this S1′ pocket unfavourable steric interactions at the Asn218-Tyr219 peptide backbone are also identified, which is causing rigid S1′ directed substituents to have less favourable MMP-8 affinity, as observed, for example, for **56** with an IC_{50} value of 500 nM.

The presence of the Arg222 side chain at the bottom of S1′ impose restrictions on the tolerable size of ligands, as it cannot freely rotate. This size-related effect is exemplified in 2-arylsulfonyl-1,2,3,4-tetrahydro-isoquinoline-3-carboxylates with different phenoxyphenyl substituents at R2 directed towards S1′. While compound **52** without substitution at this biarylether moiety shows an IC_{50} value of 9 nM against MMP-8, any additional substitution causes the affinity to decrease: **68** (4-chloro substitution: 20 nM), **81** (4-dimethylamino substitution: 30 nM), and **85** (4-(methylamido) substitution: 40 nM).

Table 1. Selected 2-arylsulfonyl-1,2,3,4-tetrahydroisoquinoline-3-carboxylates and hydroxamates as inhibitors of the matrix metalloproteinase MMP-8 to derive a structure–activity relationship

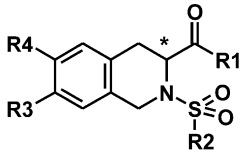

No.[a]	Isomer	R1	R2	R3	R4	MMP-8 IC_{50} (nMol/l)
8	R	NH–OH	4-Phenoxybenzene	H	H	2
9	R	NH–OH	Benzene	H	H	20
20	S	NH–OH	4-Methoxybenzene	H	H	1000
21	R	NH–OH	4-Methoxybenzene	H	H	4
22	R	NH–OH	4-(4-Dimethylaminophenoxy)-phenyl	H	H	2
23	R	NH–OH	4-Biphenyl	H	H	2
29	R	OH	4-Methoxybenzene	H	H	7000
30	R	NH–OH	4-Methoxybenzene	NH_2	H	2
36	R	NH–OH	4-Morpholinobenzene	H	H	100
48	R	OH	4-Methoxybenzene	NH_2	H	2000
49	R	OH	4-Chlorobiphenyl	H	H	5
50	R	NH–OH	4-Chlorobiphenyl	H	H	3
52	R	OH	4-Phenoxybenzene	H	H	9
56	R	OH	2-Dibenzofuran	H	H	500
60	R	OH	4-Chlorobiphenyl	NH_2	H	7
62	R	OH	4-Biphenyl	H	H	10
63	R	OH	4-(4-Dimethylaminophenyl)-benzene	H	H	1
67	S	OH	4-Chlorobiphenyl	H	H	3000
68	R	OH	4-(4-Chlorophenoxy)-benzene	H	H	20
80	R	OH	2-(2H-[1,2,3]triazole)	H	H	90
81	R	OH	4-(4-Dimethylamino)-phenoxybenzene	H	H	30
85	R	OH	4-(N-Methyl-4-phenoxy-benzamide)	H	H	40
89	R	COOH	4-(4-Trifluoromethyl)-biphenyl	H	H	10

[a]The compound ID numbering refers to ref 19.

If the distal ring in S1′ directed biaryl-substituents is polar or sterically demanding, the biological activity also decreases. This is exemplified by compound **80** with a distale triazole ring system (90 nM) and compound **36** with a morpholine system (100 nM). This latter finding is even more surprising, as the parent Tic scaffold carries a hydroxamate in **36**. In contrast, this detrimental effect for affinity is not so pronounced when changing the *para* substitution in the distal aromatic ring. The polar 4-dimethylamino-biphenyl-derivative **63** shows very good activity due to additional favourable interactions of the basic group, whereas a lipophilic CF_3 (**89**, 10 nM) is disfavoured compared to the sterically less demanding 5-chloro derivative **49** (5 nM).

Finally, the preferred stereochemistry of the 1,2,3,4-tetrahydroisoquinoline ring is R, while chirality inversion lead to a loss of binding affinity. This inversion of chirality is causing the Tic aromatic ring to move away from a favourable region for hydrophobic protein–ligand interactions. This location at the MMP-8 protein surface agrees perfectly to favourable interactions of a hydrophobic probe atom to the binding cavity identified using the program GRID.[22] This affinity difference might be caused by hydrophobic interactions to the plane of the His207 imidazole. While, for example, the 4-chlorobiphenylsulfonyl-substituted Tic derivative **49** shows an IC_{50} value of 5 nM in (*R*)-configuration, its enantiomer **67** is much less active (3000 nM, *S*-configuration).

This combined analysis leads to a detailed understanding of relevant protein–ligand interactions for further ligand design. In addition, the availability of a validated and predictive 3D-QSAR model was the basis for rank-ordering novel synthetic candidates. These 3D-QSAR results[19] based on CoMFA and CoMSIA analyses allow to focus on those regions, where steric, electronic or hydrophobic effects play a dominant role in ligand–receptor interactions.

Pharmacokinetic Studies

To obtain information on oral bioavailability, relevant in vivo pharmacokinetic (PK) studies in rabbits were conducted for selected compounds. The pharmacokinetic profiles discussed below result from analysis of rabbit blood plasma levels after oral administration of the corresponding inhibitor. The maximum drug concentration in plasma (Cmax), the halflife ($t_{1/2}$) and area under the curve (AUC) from those studies were compared to identify the optimal candidate. Relevant pharmacokinetic parameters for selected compounds after the first design cycle plus newly designed analogues from the second cycle are summarized in Table 2. The following section provides a discussion of structural elements which are correlated with oral bioavailability in this series, based on a comparative analysis of data from Table 2.

In order to arrive at inhibitors with acceptable bioavailability, the use of 1,2,3,4-tetrahydro-isoquinoline-3-carboxylates was seen as prerequisite, while a compensation for the loss of MMP-8 binding affinity was achieved by appropriate substituents within the S1′ pocket. Although the parent compound from the 1,2,3,4-tetrahydroisoquinoline-3-carboxylate series **29** with 4-methoxybenzene sulfonyl substitution in S1′ shows low MMP-8 activity, excellent oral bioavailability indicated by maximum plasma levels (Cmax) of 188 μg/mL from rabbit plasma after oral administration of 100 mg/kg was detected. On the other hand, the corresponding hydroxamic acid derivative **21** is a potent MMP-8 inhibitor without significant oral bioavailability: at a dose of 100 mg/kg maximal plasma levels (Cmax) of only 2.3 μg/mL were detected. Please note that only for these compounds, the corresponding studies were conducted with doses of 100 μg/kg, while for all other candidates below, this dose was reduced to 15 mg/kg (cf. Table 2). Those unfavourable pharmacokinetic properties, apparently associated with rapid metabolism and excretion of **21**, prevented this compound from further evaluation. Similar observations were made for related hydroxamic acid derivatives (no data given). This prompted us to search for corresponding carboxylates with increased enzyme activity, while maintaining their favourable pharmacokinetic properties.

Enlargement of the S1′-directed substituent resulted in MMP-8 activity enhancement for 1,2,3,4-tetrahydroisoquinoline-3-carboxylates. In addition, oral bioavail-

Table 2. Additional data on enzyme selectivity and PK-properties of some of the most important compounds during the optimization cycles; PK-data are based on rabbit studies at 15 mg/kg po dosing (details are given in the Experimental)

Example	IC_{50} MMP-1 (nM)	IC_{50} MMP-3 (nM)	IC_{50} MMP-13 (nM)	Cmax (μg/mL)	AUC (μg/mL×h)	Remarks
21	nd	nd	nd	2.3[a]	2.3[a]	Unfavourable properties
29	nd	nd	nd	188[a]	nd[a]	Lack of MMP-8-activity
49	7000	100	40	nd	nd	Study cancelled
52	600	200	50	4.7	49.9	Selectivity versus MMP-1 not sufficient
68	2000	500	40	15.5	267	Unfavourable elimination profile
81	500	600	nd	0.3	nd	Selectivity and PK-data not sufficient
94	> 10,000	30	100	1.9	nd	Cmax not sufficient
95	> 10,000	13	10	1.6	nd	Cmax not sufficient
96	> 10,000	20	20	29	887	Best compound

nd, not determined.
[a]At 100 mg/kg.

ability could be improved after introduction of adequate ring systems within the S1′ pocket, for example the biphenyl ether substituent. The representative carboxylate **52** with this S1′ directed substitution exhibited a Cmax value of 4.7 μg/mL at a dose of 15 mg/kg in rabbits. However, this compound lacks sufficient selectivity with respect to the undesirable metalloproteinase MMP-1. Modifications at the distal phenyl ring in *para* position was found to enhance selectivity by a factor of 4 for the 4-chlorine derivative **68** with a 3-carboxylate attached to the central scaffold, while in general activity against all relevant MMPs (MMP-3, -8, -13) decreases. Nevertheless, to support the design rational, pharmacokinetic studies were conducted for this lipophilic compound, resulting in high maximum plasma levels with a Cmax value of 15.5 μg/mL at a dose of 15 mg/kg in rabbits. However, a more careful analysis revealed a non-reproducible and unfavourable elimination profile, which prevented us from additional studies on **68**.

Further variations of substituents at the distal phenyl ring in biphenyl-ether S1′ directed substituents did not further improve the pharmacokinetic profile. Although the more polar 4-dimethylaminophenyl substituent in **81** lead to increased water solubility, it shows inacceptable enzyme activity and selectivity. The pharmacokinetic

Table 3. 2-Arylsulfonyl-1,2,3,4-tetrahydroisoquinoline-3-carboxylate and-hydroxamate MMP-8 inhibitors after second design cycle

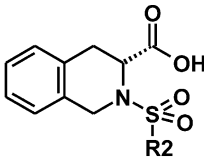

No.	R2	Isomer	^{1}H NMR (DMSO-d_6, 300 MHz)	MS (M + H)	MMP-8 IC 50 (nM)	MMP-3 IC 50 (nM)
91	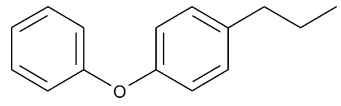	R	2.9–3.6 (4 m, 6H, CH_2); 4.6 (dd, 2H, CH_2; 4.8 (m, 1H, CH); 6.9 (dd, 4H, ar); 7.1–7.4 (m, 11H, ar)	472.6	3000	500
92	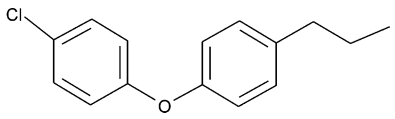	R	2.9–3.5 (3 m, 6H, CH_2); 4.32 (m, 1H, CH); 4.5; 4.72 (2 d, 2H, CH_2); 7.0 (dd, 4H, ar); 7.1 ('s', 4H, ar); 7.35 (2 d, 4H, ar)	438.2	7000	2000
93	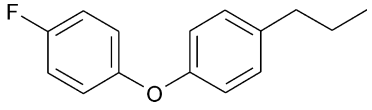	R	2.9–3.6 (4 m, 6H, CH_2); 4.65 (dd, 2H, CH_2; 4.75 (m, 1H, CH); 6.9 (d, 2H, ar); 7.0 (m, 2H, ar) 7.2 (m, 8H, ar)	456.3	2000	300
94	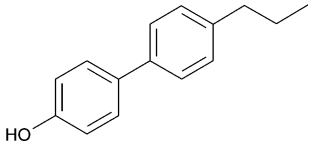	R	3.0–3.6 (m, 6H, CH_2); 4.6 (m, 3H, CH, CH_2); 6.83 (d, 2H, ar); 7.15 ('s', 4H, ar); 7.45 (d, 2H, ar); 7.47 (dd, 4H, ar); 9.5 (s, br, 1H, OH)	438.2	40	30
95	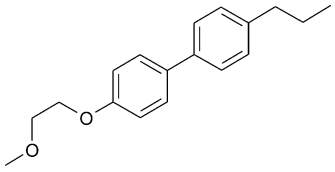	R	3.0–3.6 (m, 9H, CH_2, CH_3); 3.8 (m, 2H, CH_2); 4.11 (m, 2H, CH_2); 4.6 (m, 3H, CH, CH_2); 6.01 (d, 2H, ar); 7.15 ('s', 4H, ar); 7.30 (d, 2H, ar); 7.52 (dd, 4H, ar	496.2	30	10
96	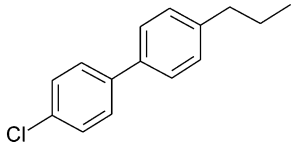	R	3.03 (m, 2H, CH_2); 3.17 ('d', 2H, CH_2); 3.52 (m, 2H, CH_2); 4.66 (dd, 2H, CH_2); 4.83 (m, 1H, CH); 7.20 (m, 4H, ar); 7.35; 7.45; 7.58; 7.66 (4 d, 8H, ar)	494.1 (+ FAB/K)	10	20

parameters of this less lipophilic compound also did not fulfill the desired profile: A Cmax value of only 0.3 μg/mL was observed in rabbits after oral administration of a dose of 15 mg/kg. The evaluation of corresponding hydroxamic acids led to similar conclusions as described above for the analogues **21**/**29**. As representative molecules of other subseries also showed insufficient pharmacokinetic properties, a new design cycle was initiated to retain MMP-8 activity and selectivity, while improving pharmacokinetic properties of the candidate molecules.

Novel MMP-8 Inhibitors from Second Design Cycle

These previously outlined SAR results were applied to design novel synthesis candidates based on the 1,2,3,4-tetrahydroisoquinoline-3-carboxylate scaffold with high affinity and improved oral bioavailability (Table 3). To take advantage of favourable hydrophobic interactions at the bottom of the S1′ specificity pocket for MMP-8 affinity, biaryl- and biarylether substituents were oriented deeper within this pocket by introducing an ethyl spacer between the aromatic moiety and the sulfonamide at the 1,2,3,4-tetrahydro-isoquinoline-3-carboxylate scaffold. Thus, a variety of substituted 2-(biphenyl-4-yl)-ethanesulfonamides were designed, evaluated by flexible docking into the MMP-8 binding pocket and CoMFA based affinity predictions. The most promising candidate molecules were synthesized and subjected to further profiling.

For ranking of virtual synthesis candidates, their MMP-8 affinities were predicted after docking using the previously reported CoMFA model[19] with 2 Å grid spacing based on 90 MMP-8 inhibitors, showing a cross-validated r^2 value of 0.569 for five PLS components and a conventional r^2 of 0.905. To demonstrate the ranking of compounds by this model, a graph of observed versus predicted biological activities[33] is shown in Figure 3B. Compounds included in the training set are indicated by dots, while a priori affinity predictions for five newly synthesized candidates with this ethyl spacer described below are indicated by crosses. All compounds were evaluated for inhibitory activities on MMP-8 and MMP-3 using an amidolytic assay previously described.[19] The chemical structures, analytical data and corresponding IC_{50}-values are summarized in Table 3.

From this design cycle, compound **96** with a 2-(4′-chloro-biphenyl-4-yl)-ethanesulfonamide side chain attached to the 1,2,3,4-tetrahydroisoquinoline-3-carboxylate scaffold has highest MMP-8 affinity (IC_{50} 10 nM, cf. Table 3). The postulated binding mode for **96** after docking into MMP-8 is displayed in Figure 3A. When comparing the experimentally determined binding mode of compound **62** with only a biaryl substituent to the postulated binding mode of this analogue, a slight movement of Arg222 at the bottom of the S1′ pocket has to be assumed in order to accommodate the larger substituent in this specificity pocket. This sidechain flexibility is reproduced by the employed docking protocol outlined below and also observed upon comparative analysis of in-house and public domain MMP-8 X-ray structures. The binding mode of **96** is characterized by a location of the hydrophobic portion of the 2-(4′-chloro-biphenyl-4-yl)-ethanesulfonamide substituent deeper in the S1′ pocket, while no unfavourable interactions close to the narrow entrance into the S1′ pocket were observed. Hence, this derivative presents another example for the observation that a loss of favourable zinc binding affinity in hydroxamates can be compensated by adequate substituents in this S1′ specificity pocket.

Additional biological and pharmacological profiling ultimatively reveals compound **96** as best member from this series. This compound is not only a potent MMP-8 inhibitor, it also shows a high predicted human absorption (>95%, as estimated from Caco-2 cell permeability assays)[34] metabolic stability in S9 liver fractions in adequate in vitro assays. No significant inhibition on a variety of cytochrome P 450 isoforms was detected in additional in vitro profiling assays.[35] Moreover, **96** shows favourable in vivo pharmacokinetic properties, as found in corresponding animal experiments. In rats (male Wistar rats) a maximal plasma concentration Cmax[36] after oral administration of 21 μg/mL was obtained with a half-life of 4 h after 15 mg/kg single oral dosing. In rabbits the observed Cmax value was 29 μg/mL, with a halflife of 29 h after administration of a

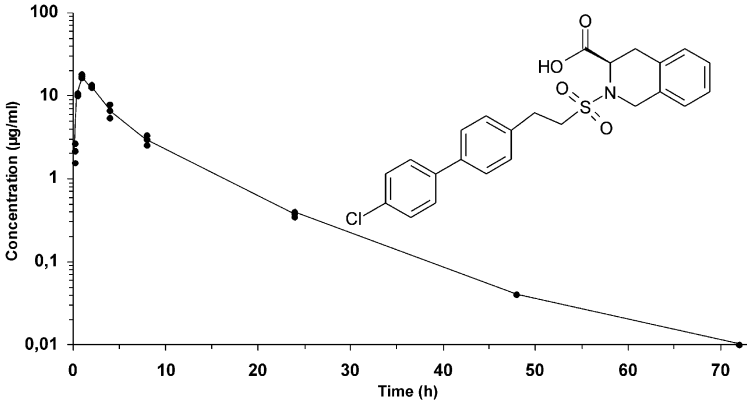

Figure 4. Mean concentration–time curve (μg/mL vs h) showing the plasma elimination profile of compound **96**. Administration of a single oral dose of 6 mg/kg in healthy beagle dogs ($n=2$; vehicle: 1% CMC, 0.05% DONSS) gave a maximal plasma concentration Cmax of 17 μg/mL, with a half life of 7 h.

single oral dose of 15 mg/kg. In all studies, 1% CMC and 0.05% DONSS[36] were used as vehicle. Monitoring was done by RP-HPLC analysis of plasma samples taken at distinct time points. Absolute bioavailabilities in both animal species after analysis of the corresponding iv experiments were determined to be 53% (rat) and 64% (rabbit). These promising pharmacokinetic properties of **96** were underlined by conducting in vivo studies in beagle dogs. Here, a Cmax value of 17 μg/mL, with a half-life of 7 h is obtained after administration of a single oral dose of 6 mg/kg (same vehicle as above), resulting in an absolute oral bioavailability of 100% after analysis of corresponding iv experiments. The pharmacokinetic profile after oral administration in dogs is shown in Figure 4 as time versus concentration graph. The maximum drug concentration in plasma (Cmax) is reached at about 1 h after single oral dosing. The graphical inspection of Figure 4 also suggests a favourable elimination profile with similar characteristics in all animal species.

The comparison of **96** to **94** and **95** suggests that the lipophilic S1′ directed substituent carrying a 4-chlorine substituent is responsible for the acceptable pharmacokinetic profile. Replacing this 4-Cl by a more polar phenolic hydroxyl group in **94** or a methoxy–ethoxy substituent in **95** still resulted in acceptable MMP-8 affinity, while lower plasma levels (Cmax values 1.9 μg/mL for **94** and 1.6 μg/mL for **95**) and shorter half-life were observed.

These pharmacokinetic data of **96** let us to consider this compound as a promising candidate for further biological profiling towards the treatment of MMP-related diseases. Hence, the modification of an unwanted chemical functionality, which nevertheless is required for high binding affinity to the binding cavity of MMP-8, against a more tolerable but weaker substrate was achieved by a combination of structure-based design, 3-D-QSAR-studies and pharmacokinetic profiling.

Conclusion

The systematic evaluation of nonpeptidic 2-arylsulfonyl-1,2,3,4-tetrahydro-isoquinoline-3-carboxylates and-hydroxamates as inhibitors of the matrix metalloproteinase MMP-8 led us to establish their structure–activity relationship. In combination with a high-resolution X-ray structure for one derivative plus a predictive 3D-QSAR model to explain affinity towards MMP-8, a better understanding of relevant protein–ligand interactions responsible for high affinity ligands was generated. This knowledge provided essential information for a subsequent structure-based design cycle to arrive at inhibitors with an improved pharmacokinetic profile and high activity against the target enzyme MMP-8. In this process the 3D-QSAR model was successfully applied to rank-order candidates during lead optimization. Although carboxylates exhibit weaker zinc binding properties than hydroxamates, they are known to show better oral bioavailability and are less prone to metabolic degradation. It was possible to compensate the expected loss of binding affinity after replacement of hydroxamates against carboxylates by adequate choice of elongated S1′ directed substituents. The novel MMP-8 inhibitors carrying substituted 2-(biphenyl-4-yl)-ethanesulfonamides attached to the 1,2,3,4-tetrahydro-isoquinoline scaffold did not only result in highly active compounds, but also in compounds with improved pharmacokinetic properties. In particular, compound **96** shows an interesting in-vitro profile and also exhibits significant oral bioavailability in three animal species. Hence, a novel class of orally available MMP-inhibitors emerged from this study. This iterative procedure towards the discovery of novel MMP-8 inhibitors with high affinity and good pharmacokinetic properties was only possible after a successful combination of medicinal chemistry, structure-based design, reliable affinity predictions using 3D-QSAR models and pharmacokinetic profiling. It is expected that additional new inhibitor classes directed towards MMP-8 may emergy from the combined application of these techniques for therapy of several MMP-related diseases.

Experimental

Enantiomerically pure 1,2,3,4-tetrahydroisoquinoline-3-carboxylic acid is commercially available (e.g., Nutrasweet company). Sulfonic acid chlorides are commercially available or were prepared by literature procedures. ^{1}H NMR spectra were recorded at room temperature on a 200 MHz spectrometer from Varian or a 400 MHz spectrometer from Bruker with tetramethylsilane (TMS) as internal standard in DMSO-d_6. Final products were characterized by NMR and mass spectroscopic methods (FAB-, ESI-MS). Temperature data in degrees Celsius, rt means room temperature (22–25 °C). Melting points were determined with a Büchi capillary melting-point apparatus, and they are uncorrected. All abbreviations are explained or correspond to conventions.

Synthesis

2-(4-Chlorobiphenylethanesulfonyl)-1,2,3,4-tetrahydro-isoquinoline-3-carboxylic acid (96) (cf. Scheme 2). 1-(2-Bromoethenone)-4-(4-chlorophenyl)-benzene 96a. To a stirred suspension of $AlCl_3$ (34.7 g, 0.26 mol) and bromoacetyl bromide (25.2 g, 0.125 mol) in 400 mL CS_2 4-chlorobiphenyl (23.6 g, 0.125 mol) was gradually added at 0° C and then heated at reflux temperature for 3 h. The reaction mixture was slowly added to crushed ice, extracted with EtOAc and washed with a saturated aqueous $NaHCO_3$ solution and water. The organics were dried over anhydrous sodium sulfate and concentrated under reduced pressure. The residue was recrystallized from dichloromethane. Yield: 24.2 g (62% of theory). Mp: 127–128 °C; ^{1}H NMR: (300 MHz) 5.0 (s, 2H, CH_2); 7.5–8.1 (4 d, 8H, ar); MS: 311.1 (M + H).

4-Chlorobiphenylethane bromide 96b. To a stirred suspension of $AlCl_3$ (20.0 g, 0.15 mol) in dichloromethane (500 mL) was added tert-butylamine borane (27.5 g,

0.31 mol) at 0 °C. After stirring the resulting mixture at 0° C for 15 min a solution of the bromo ketone **96a** (16.0 g, 50 mmol) in dichloromethane (150 mL) was added and stirred at 0 °C for additional 4 h. Cold dilute HCl (1 N, 30 mL) was added dropwise to the reaction mixture, following by extraction with EtOAc. The combined organic extracts were washed with dilute HCl and then with brine. The concentration of the organic extracts gave an oil which was purified by flash chromatography on silica. Yield: 15 g (quant). Mp: 142 °C; ^{1}H NMR: (300 MHz) 3.2; 3.78 (2 t, 4H, CH_2); 7.4–7.7 (4 d, 8H, ar); MS: 296.2 (M + H).

Sodium salt of 4-chloro-biphenylethane sulfonic acid 96c. Compound **96b** (14.8 g, 50 mmol) was dissolved in a mixture of ethanol and water (1:1, 200 mL). After adding sodium sulfite (9.5 g, 75 mmol) and tetrabutylammonium jodide (1.8 g, 5 mmol) the mixture was heated at reflux temperature for 16 h. From a small amount of a solid was decanted, the solvent partly removed and on cooling the product crystallizes. It was filtered off, recrystallized from MeOH/H_2O and dried in vacuo. Yield: 13.9 g (94% of theory). ^{1}H NMR: (300 MHz) 2.6; 2.95 (2 m, 4H, CH_2); 7.3–7.7 (4 d, 8H, ar).

4-Chloro-biphenylethanesulfonyl chloride 96d. To a suspension of the sodium sulfonate **96c** (4.8 g, 15 mmol) in phoshorus oxychloride (50 mL) was added phoshorus pentachloride (3.2 g, 15 mmol). After heating at 60 °C for 6 h the solution was poured into ice water after methylene chloride was added. Saturated sodium hydrogen carbonate solution was added to neutralize the mixture, the organic phase was separated, dried and the solvent removed. Yield: 5 g (quant). ^{1}H NMR: (300 MHz) 2.9 (m, 4H, CH_2); 7.3–7.7 (4 d, 8H, ar).

2-(4′-Chloro-biphenyl-4-ethylsulfonyl)-1,2,3,4-tetrahydroisoquinoline-3-carboxylic acid (96). To a suspension of D-Tic (1.4 g, 8 mmol) in 30 mL dry acetonitrile bis-(trimethylsilyl) trifluoroacetamide (2.3 g, 9 mmol) was added under Ar and then refluxed for 2 h. To this solution, 4-chloro-biphenylethanesulfonyl chloride **96d** (2.84 g, 9 mmol) in 30 mL acetonitrile was added and refluxed for 3 h. After cooling to rt, 9 mL 1 M HCl was added to the reaction mixture and stirred for 1 h. The solvent was removed, water and chloroform added, the organic phase separated and dried. After removal of the solvent the product was precipitated from toluene and recrystallized twice from MeOH. Yield: 1.1 g (30 of theory; purity >98%; mother lipuors could be recycled to a total yield of 65% with a purity >94%). Mp: 211–212 °C; ^{1}H NMR: (300 MHz) 3.0–3.6 (3 m, 6H, CH_2); 4.6 ('q' 2H, CH_2); 4.82 (t, 1H, CH); 7.2–7.7 (mm, 12H, ar); MS: (M + H).

2-(4-Methoxybenzenesulfonyl)-7-amino-1,2,3,4-tetrahydroisoquinoline-(*R*)-3-(*N*-hydroxy)carboxamide (30). (6/7)-Nitro-1,2,3,4-tetrahydroisoquinoline-(*R*)-3-carboxylic acid 30a/b. 100 g of 1,2,3,4-tetrahydroisoquinoline-3-carboxylic acid (564 mmol) were dissolved or suspended in 500 mL of sulfuric acid (98%, d 1.84) at −10 °C and cooled to −30 °C. 59 g (584 mmol) of potassium nitrate, dissolved in 200 mL of sulfuric acid and cooled to 0 °C, were then added dropwise during 1.5 h. The internal temperature should not exceed −10 °C in this process. After completion of the addition of nitrate, the mixture was additionally stirred for 10 min at −10 °C and for 1 h without external cooling. The mixture was poured onto ice and neutralized with concentrated aqueous ammonia solution with cooling; consumption approximately 1.8 L of the 25% strength solution. Before filtering off the precipitating amino acid, the mixture was diluted with the same volume of water. The solid obtained was again suspended in water and filtered off to remove residual ammonium salts. It was washed with plenty of cold water and dried at 60 °C under reduced pressure. Yield: 110.1 g (88% of theory). Mp: from 245 °C (slow discoloration), 272–275 °C (melts with decomposition); ^{1}H NMR: (400 MHz, DCl/D_2O) 3.05 (dd, 1H, 7-isomer); 3.30 (2 dd, superimposed, 2H, 6- and 7-isomer); 3.44 (dd, 1H, 6-isomer); 4.25 (m, 3H); 7.20; 7.80 (2 m, 3H); proportion of 6-isomer: 13%. Elemental analysis: C 53.9 (theor. 54.06), H 4.50 (theor. 4.55), N 12.6 (theor. 12.61); IR: 1640 (s), 1540 (s), 1400 (s), 1350 (s) cm^{-1}.

***tert*-Butoxycarbonyl-(6/7)-nitro-1,2,3,4-tetrahydroisoquinoline-(*R*)-3-carboxylic acid.** 13.3 g (59.9 mmol) of the nitro imino acid mixture **30a/b** were dissolved or suspended in 300 mL of dioxane/water 1:1; 13.1 g (60 mmol) of di-*tert*-butyl dicarbonate and 12.72 g (120 mmol) of sodium carbonate was added and the mixture was stirred at room temperature for 16 h. The dioxane was then distilled off on a rotary evaporator and the residual aqueous suspension covered with a layer of 200 mL of ethyl acetate. The mixture was cooled to 5 °C, acidified to pH 3 (1 N HCl) and the organic phase is separated off. It was then washed twice with saturated NaCl solution and dried over sodium sulfate. After filtering off the drying agent, the filtrate was evaporated under reduced pressure. Yield: 18.1 g (94% of theory). Purity/isomer distribution: HPLC determination: Nucleosil RP 18, 125×4 mm, 254 nm, acetonitrile/0.1 M phosphoric acid 5:95–70:30; 6-isomer: retention time 14.19 min, 7-isomer: retention time 14.72 min. Ratio approximately 1:9; purity: 99.0%; ^{1}H NMR: (200 MHz) 1.4 (2 s, 9H); 3.3 (m, 2H); 4.4–5.0 (3 m, 3H); 7.4–8.2 (5 m, 3H); 12.7 (s, 1H).

Dicyclohexylammonium 2-*tert*-butoxycarbonyl-7-nitro-1,2,3,4-tetrahydroisoquinoline-(*R*)-3-carboxylate 30c. To separate the regioisomers, 10 g of the mixture of the Boc-iminoacids were dissolved in 300 mL of ethyl acetate and then treated at room temperature with 1 equiv (6.2 mL) of dicyclohexylamine in 10 mL of ethyl acetate. In the cold, after addition of n-heptane, the dicyclohexylammonium salt slowly crystallizes out, was filtered off after 16 h and dried. After two further recrystallizations, the proportion of the 6-isomer was less than 1.0% with a total purity of greater than 99%. Further material can be obtained from mother liquors. Yield: 6.1 g (1st fraction). Purity/isomer distribution: HPLC determination: Nucleosil RP 18, 125×4 mm, 254 nm, acetonitrile/0.1 M phosphoric acid 5:95 to 70:30; 6-isomer: retention time 13.51 min, 7-isomer: retention time 14.23 min. Ratio >1:99. ^{1}H NMR: (200 MHz) 0.9–1.9 (several m, about

30H); 2.7–3.05; 3.4; 4.6 (5 m, about 5H); 7.4; 8.0 (2 m, 3H). Specific rotation: −23.6° (MeOH, $c = 1$).

2-*tert*-Butoxycarbonyl-7-nitro-1,2,3,4-tetrahydroisoquinoline-(*R*)-3-carboxylic acid. To liberate the protected amino acid **30c**, the DCHA salt was dissolved in ethyl acetate and extracted by shaking with an excess of aqueous, 10% strength citric acid solution. The organic phase was extracted by shaking with saturated NaCl solution, dried over sodium sulfate and evaporated under reduced pressure. Yield: 87–95%. ^{1}H NMR: The characteristic signals of dicyclohexylamine are absent. The compound liberated was immediately further processed.

7-Nitro-1,2,3,4-tetrahydroisoquinoline-(*R*)-3-carboxylic acid hydrochloride 30d. 0.5 g of the above mentioned compound (1.55 mmol) were treated with 19 mL of HCl in ether and the mixture was stirred at rt for 30 min, evaporated to dryness, coevaporated several times with toluene and dried under reduced pressure. Yield: 0.385 g (96% of theory). ^{1}H NMR: (200 MHz) 3.2–3.6 (m, 2H); 4.3–4.6 (m, 3H); 7.6 (d, 1H); 8.1 (dd, 1H); 8.3 (d, 1 h); 10.5 (s, br., 1H); MS: 223.1 (M + H). Specific rotation: + 143.5° ($c = 1$, MeOH).

2-*tert*-Butoxycarbonyl-7-amino-1,2,3,4-tetrahydroisoquinoline-(*R*)-3-carboxylic acid. 38 g of the regiopure Boc-nitro compound (117 mmol) were hydrogenated in a Parr apparatus at rt and a slight excess pressure for 7 h with 2 g of 10% Pd on C in methanol. After evaporating the solvent, the residue was washed with diisopropyl ether and recrystallized from water/ethanol and finally dried under reduced pressure. Yield: 33 g (95% of theory). ^{1}H NMR: (200 MHz) 1.4 (2 s, 9H); 2.9 (m, 2H); 4.2–4.8 (several m, 3H); 6.4 (m, 2H); 6.8 (m, 1H). MS: 293.1 (M + H). Specific rotation: + 28.33° ($c = 1$, methanol).

2-*tert*-Butoxycarbonyl-(6/7)-amino-1,2,3,4-tetrahydroisoquinoline-(*R*)-3-carboxylic acid. For reduction of the Boc-nitro-mixture, the procedure was as above. The crude product was evaporated under reduced pressure. ^{1}H NMR: (200 MHz) 1.4 (2 s, 9H); 2.9 (m, 2H); 4.2–4.8 (several m, 3H); 6.4 (m, broad, 2H); 6.8 (m, 1H). MS: 293.1 (M + H).

2-*tert*-Butoxycarbonyl-7-amino-1,2,3,4-tetrahydroisoquinoline-(*R*)-3-carboxylic acid (alternative process for separation of regioisomers). The isomer mixture from the above mentioned example was treated with a small amount of acetonitrile at boiling heat. After cooling, it was filtered off. This treatment is carried out 2–3 times. ^{1}H NMR: (200 MHz) 1.4 (2 s, 9H); 2.9 (m, 2H); 4.2–4.8 (several m, 3H); 6.4 (m, 2H); 6.8 (m, 1H); no difference from Example 6. MS: 293.1 (M + H). Specific rotation: + 28.13° ($c = 1$, methanol).

7-Amino-1,2,3,4-tetrahydroisoquinoline-(*R*)-3-carboxylic acid dihydrochloride. 0.5 g (1.7 mmol) of the Boc-protected amino imino acid were treated with HCl in ether for 30 min at rt. After evaporating under reduced pressure, the residue is coevaporated with toluene and residual solvent removed in vacuo. Yield: 0.41 g (91% of theory). ^{1}H NMR: (200 MHz) 3.0–3.5 (m, 2H); 4.2–4.5 (m, 3H); 7.1–7.4 (2 m, 3H); 10.0 (s, broad, 1H). MS: 193.0 (M + H). Specific rotation: + 86.3° ($c = 1$, methanol).

2-(4-Methoxybenzenesulfonyl)-7-amino-1,2,3,4-tetrahydroisoquinoline-(*R*)-3-(N-hydroxy)carboxamide (30). As outlined in Scheme 3 7-nitro-1,2,3,4-tetrahydroisoquinoline-(*R*)-3-carboxylic acid hydrochloride was transformed to the sulfonamide under standard Schotten–Baumann conditions followed by reduction of the nitro group to the amino group (as outlined above, resulting in compound **48** in Table 1) and introduction of the Boc protective group (described above, resulting in compound **30e**), all steps are giving the products in very high yields each (cf. Scheme 3). To prepare the hydroxamic acid, 10 g (22 mmol) of 2-(4-methoxybenzenesulfonyl)-7-(*tert*-butoxycarbonyl)-amino-1,2,3,4-tetrahydroisoquinoline-(*R*)-3-carboxylic acid 30e was dissolved in 100 mL of THF, cooled to −15 °C and treated successively with 2.1 mL (22 mmol) of ethyl chloroformate, 4.8 mL (44 mmol) of *N*-methylmorpholine and, after 45 min at this temperature, with 13.5 mL (110 mmol) of *O*-trimethylsilylhydroxylamine. The mixture was additionally stirred for 3 h at rt, the solvent was removed under reduced pressure, the residue taken up in ethyl acetate and extracted by shaking successively with 10% strength citric acid solution, 10% sodium carbonate solution and saturated NaCl solution, dried over sodium sulfate and evaporated in a rotary evaporator, and solvent residues were removed. 2.6 g of this compound (total yield 9.1 g) was purified by silica gel chromatographic, resulting in example **30** (Table 1); this compound was then treated with 50 mL of HCl in diethyl ether and the mixture was stirred at rt for 30 min. It was then evaporated under reduced pressure and the residue was coevaporated with toluene. Yield: 1.97 g (89% of theory). ^{1}H NMR: 2.75 (m, 2H); 3.8 (s, 3H); 4.40 (m, 3H); 6.9–7.3 (m, 3H); 7.0; 7.7 (2 d, 4H); 8.8; 9.3; 10.7 (3 s, 3H).

Compound **60** was prepared accordingly.

2-(4′-Dimethylamino-biphenyl-4-sulfonyl)-1,2,3,4-tetrahydro-isoquinoline-3-carboxylic acid hydrochloride (63). 4-Dimethylaminobiphenyl 63a. 10.15 g (60 mmol) 4-aminobiphenyl was dissolved together with 10.09 g (80 mmol) of dimethylsulfate in 120 mL tetrahydrofurane under stirring, 11.06 g (80 mmol) of potassium carbonate, dissolved in 100 mL of water were slowly added and stirring is continued until completion of the reaction (ca. 24 h, TLC control). After addition of ethyl acetate, the phases were separated, the aqueous phase was reextracted and the combined organic phases were washed with water and brine, dried over sodium sulfate and evaporated under reduced pressure. Purification from byproducts (monoalkylated and quat. ammonium) was performed by flash-chromatography on silica gel (ethyl acetate/petrol ether 1:9). Yield: 6.9 g (58.3% of theory).

4′-Dimethylamino-biphenyl-4-sulfonic acid 63b. 6.8 g (43.5 mmol) of compound **63a** was dissolved in 30 mL of concd sulfuric acid, and heated to 130 °C, resulting in a deep purple solution. After 30 min of stirring at

130 °C the mixture was cooled to rt and poured into 200 mL of ice-water. The product was isolated by filtration, carefully washed with water finally and dried in vacuo. Yield: 6.5 g (68% of theory).

4′-Dimethylamino-biphenyl-4-sulfonyl chloride 63c. 0.28 g (1 mmol) of **63b** was dissolved in 1 mL of phosphorus oxycloride and 0.21 g (1 mmol) phosphorus pentachloride. On heating to 100 °C, the product dissolved under gas evolution. After 5 h, the reaction was complete (HPLC control). The reaction mixture was poured into ice water and the pH adjusted to 8 (sodium bicarbonate). The product was isolated by repeated extraction with dichloromethane, washing with water and brine, then evaporation to dryness under reduced pressure. Yield: 0.25 g (84.5% of theory).

2-(4′-Dimethylamino-biphenyl-4-sulfonyl)-1,2,3,4-tetrahydro-isoquinoline-(*R*)-3-carboxylic acid hydrochloride (63). 0.11 g (0.6 mmol) of 1,2,3,4-tetrahydroisoquinoline-(*R*)-3-carboxylic acid was suspended in 30 mL tetrahydrofurane, 0.21 g (0.7 mmol) of 63c and then 0.28 g (2 mmol) of potassium carbonate, dissolved in 15 mL water under intensive stirring at rt. After 24 h, the reaction was complete (HPLC control). The pH was adjusted to 4 using aqueous citric acid, the product was extractet with ethyl acetate. The organic phase was washed with water and concd sodium chloride solution, then evaporated to give an oily residue. Trituration with methyl-*tert*-butylether resultes in 0.16 g (61.1% yield) of an amorphous product (mp 194–196 °C). This product was transferred into the hydrochloride salt by dissolving 100 mg in 5 mL tetrahydrofurane, adding 0.3 mmol of an 1 N HCl solution in diethylether and then slowly methyl-*tert*-butylether until completion of crystallization. The final product was isolated by filtration and dried in an vacuum oven at 40 °C. Yield: 85 mg (46% of theory). ^{1}H NMR (MeOH-d_4): 3.05–3.25 (m, 2H, CH_2 and s, 6H, NMe_2), 4.5–4.75 (dd, 2H, $\underline{CH_2}$–CHN), 4.95 (m, 1H, CHN), 7.05–7.2 (m, 4H, ar), 7.45–8.0 (m, 8H, ar).

2-(4-[1,2,3]Triazol-2-yl-benzenesulfonyl)-1,2,3,4-tetrahydro-isoquinoline-(*R*)-3-carboxylic acid (80). 2-Phenyl-2H-[1,2,3]-triazole 80a. The synthesis was performed in close analogy to ref 37. A mixture of 2 g (8.4 mmol) glyoxyl-bis-phenylhydrazone and 5.5 g (22 mmol) $CuSO_4 \times 5H_2O$ in water were heated to 75–80 °C under stirring for 6.5 h and then steam-distilled to remove from salts and byproducts. The triazole-water phase is saturated with NaCl and the product extracted twice with diethylether. The combined organic phase was washed with 10% aqueous HCl and water, dried and evaporated under reduced pressure. Yield: 1.15 g (94% of theory).

4-[1,2,3]Triazol-2-yl-benzenesulfonyl chloride 80b. 1.1 g (7.6 mmol) of step 1 compound 80a was chlorosulfonated using 10 equivalents of chlorosulfonic acid according to ref 40. Yield: 1.3 g (70.4% of theory).

2-(4-[1,2,3]Triazol-2-yl-benzenesulfonyl)-1,2,3,4-tetrahydro-isoquinoline-(*R*)-3-carboxylic acid (80). 0.8 g (4.5 mmol) of 1,2,3,4-tetrahydroisoquinoline-(*R*)-3-carboxylic acid was suspended in 30 mL tetrahydrofurane and 10 mL water, 1.21 g (5 mmol) of step 2 compound and then slowly 5 mL 1 N of sodium hydroxide solution was added under intensive stirring at rt. After 20 h, the reaction was complete (HPLC control). The pH was adjusted to 2 using aqueous HCl and the product was twice extractet with ethyl acetate. The organic phase was washed with aqueous sodium bicarbonate and concd sodium chloride solution, then partly evaporated and filtered over silica gel for decolorization. After removal of ethyl acetate under reduced pressure, the crude product was taken up in a small volume of methanol, treated in a ultrasonic bath for several min, then isolated by filtration and dried in vacuo. Yield: 1.05 g (60.7% of theory). ^{1}H NMR (DMSO-d_6): 3.0–3.2 (m, 2H, CH_2), 4.45–4.75 (dd, 2H, $\underline{CH_2}$-CHN), 4.9 (m, 1H, CHN), 7.05–7.25 (m, 4H, ar), 8.05 (AA′, 2H, ar), 8.15–8.3 (m, 4H, ar and triazole).

Enzyme assays

The catalytic domain of human recombinant MMP-8 (hMMP-8cd; Gly^{99}-Gln^{271}; M_r 19.9 kD) was obtained as described previously,[38] biological activities were determined in 96 well titer plate format in a luminescence spectrometer (LS 50B, Perkin-Elmer, Langen, FRG) using the quenched fluorigenic substrate[39] (7-methoxycoumarin-4-yl) acetyl-Pro-Leu-Gly-Leu-3-(2′,4′-dinitrophenyl)-L-2,3-diaminopropionyl-Ala-Arg-NH_2 [λ 328 nm (ex)/λ 393 nm (em)]. Each well contained 70 μL of buffer (0.1 mol/l Tris–HCl, pH 7.5; 0.1 mol/L NaCl; 0.01 mol/L CaCl2; 0.05% Brij 35), 10 μL of enzyme, and 10 μL of drug in 19% DMSO. After preincubation for 15 min at rt the reaction was started by addition of 10 μL of substrate (1 mmol/L in 10% DMSO). The initial velocity of the enzymatic reaction was determined without ligand (=100%) and with seven different ligand concentrations, ranging from 10^{-4} to 10^{-10} mol/L. Each measurement was done in duplicate to ensure statistically significant results ($p < 0.05$). The ligand-dependent inhibition of the intial velocity was plotted, and the IC_{50} values were determined using standard software.

Computational procedures

All modelling work was performed using the program SYBYL,[40] energy calculations were based on the TRIPOS 6.0 force field[41] including Gasteiger–Marsili charges.[42] Conformations of ligands and protein–ligand complexes were minimized using quasi-Newton–Raphson (BFGS) or conjugate gradient (CG) procedures. For docking, X-ray structures of catalytic domains of MMP-8 provided starting geometries. After analysis of protein–ligand interactions using the program GRID,[22] candidate molecules were manually docked into the active site. Subsequently the protein–ligand complex was minimized treating all ligand atoms plus all protein residues within a sphere of 4 Å as flexible, while the remaining receptor was only used to compute non-bonded interactions. All other compounds were built

accordingly, docked into MMP-8 and minimized. Some candidate molecules were further optimized using a genetic algorithm docking procedure implemented in the program FlexiDock,[28] which did not result in alternative binding modes. Scoring of novel synthetic candidates was done by inspection of the complementarity of protein–ligand interactions after minimization plus quantitative affinity predictions using 3D-QSAR models reported in ref 19.

Rabbit PK studies

Rabbit PK studies were performed using a standard drug concentration of 15 mg drug/kg animal body weight in 0.1 M sodium phosphate buffer solution pH 8.0, except if noted otherwise. Data sampling was performed by taking blood samples from the ear vein into heparinized syringes according to the following time schedule: predose (=0), 30, 60, 120, 180, 240, 360 and 1440 min post administration. Subsequently all plasma samples were treated by combining 500 μL plasma with 50 μL acetonitril and 50 μL internal drug standard solution with 100 μL 1 N HCl and 2.5 mL dichloromethane. The internal drug standard solution was prepared by generating a 50 mL solution in acetonitril containing 0.5 mMol drug substance. The subsequent extraction of the organic layer was done for 15 min by using a CENCO mixer. After centrifugation (3500 rpm), the organic layer was dried under a gentle stream of nitrogen at 40 °C. The residue was taken up in 100 μL acetonitril and 100 μL water. HPLC: Merck I-6200A and L-7200 Autosampler; processing: Waters Maxima chromatography workstation; column: Nucleosil C18; column size: 125×4 mm; particle size: 5 μm; detection: UV–absorbance (246 nm) GAT LCD 503; flow rate: 1.5 mL/min; inj. solut.: 200 μL acetonitril + 100 μL water; inj. vol.: 20 μL; limit of detection: <10 ng/mL plasma; elution: start with: 10% acetonitril/90% 0.1 M H3PO4; go to 70% acetonitril after 10 min, keep constant for 5 min. The chemical purity of the compound was usually >96% and checked immediate prior to performing the in vivo PK study.

Acknowledgements

We thank H. Schreuder, V. Wehner, S. Ruf and B. Pirard (all Aventis Pharma) for helpful discussions.

References and Notes

1. (a) Woessner, J. F., Jr. *FASEB J*. **1991**, *5*, 2145. (b) Birkedal-Hansen, H.; Moore, W. G. I.; Bodden, M. K.; Windsor, L. J.; Birkedal-Hansen, B.; DeCarlo, A.; Engler, J. A. *Crit. Rev. Oral Biol. Med.* **1993**, *4*, 197. (c) Murphy, G.; Docherty, A. J. P. *A. J. Res. Cell. Mol. Biol.* **1992**, *7*, 120. (d) Matrisian, L. M. *Trends Genet*. **1990**, *6*, 121.
2. Lohmander, L. S.; Hoerrner, L. A.; Lark, M. W. *Arthrit. Rheum*. **1993**, *36*, 181.
3. Murphy, G.; Hembry, R. M. *J. Rheumatol*. **1992**, *19*, 61.
4. Peress, N.; Perillo, E.; Zucker, S. *J. Neuropathol. Exp. Neurol*. **1995**, *54*, 16.
5. Bode, W.; Reinemer, P.; Huber, R.; Kleine, T.; Schnierer, S.; Tschesche, H. *EMBO J*. **1994**, *13*, 1263.
6. (a) Nishino, N.; Powers, J. C. *Biochemistry* **1979**, *18*, 4340. (b) Powers, J. C.; Harper, J. W. In *Proteinase Inhibitors*; Barrett, A. J., Salvesen, G., Eds.; Elsevier: Amsterdam, New York, Oxford, 1986; p 219. (c) Johnson, W. H.; Roberts, N. A.; Borkakoti, N. *J. Enzyme Inhib*. **1987**, *2*, 1. (d) Zask, A.; Levin, J. I.; Killar, L. M.; Skotnicki, J. S. *Curr. Pharm. Design* **1996**, *2*, 624.
7. Reinemer, P.; Grams, F.; Huber, R.; Kleine, T.; Schnierer, S.; Pieper, M.; Tschesche, H.; Bode, W. *FEBS Lett*. **1994**, *338*, 227.
8. Stams, T.; Spurlino, J. C.; Smith, D. L.; Wahl, R. C.; Ho, T. F.; Qoronfleh, M. W.; Banks, T. M.; Rubin, B. *Nature Struct. Biol*. **1994**, *1*, 119.
9. Grams, F.; Reinemer, P.; Powers, J.; Kleine, T.; Pieper, M.; Tschesche, H.; Huber, R.; Bode, W. *Eur. J. Biochem*. **1995**, *228*, 830.
10. Grams, F.; Crimmin, M.; Hinnes, L.; Huxley, P.; Pieper, M.; Tschesche, H.; Bode, W. *Biochemistry* **1995**, *34*, 14012.
11. Betz, M.; Huxley, P.; Davies, S. J.; Mushtaq, Y.; Pieper, M.; Tschesche, H.; Bode, W.; Gomis-Rueth, F. X. *Eur. J. Biochem*. **1997**, *247*, 356.
12. Schlechter, I.; Berger, A. *Biochem. Biophys. Res. Commun*. **1967**, *27*, 157.
13. PDB-files from Protein Database (National Brookhaven Laboratories): 1MMB, 1MNC, 1KBC, 1JAN, 1JAO, 1JAP and 1JAQ (http://www.pdb.bnl.gov) Bernstein, F. C.; Koetzle, T. F.; Williams, G. J. B.; Meyer, E. F.; Brice, M. D.; Rodgers, J. R.; Kennard, O.; Shimanouchi, T.; Tasumi, M. *J. Mol. Biol*. **1977**, *112*, 535.
14. Cramer, R. D.; Patterson, D. E.; Bunce, J. E. *J. Am. Chem. Soc*. **1988**, *110*, 5959.
15. Clark, M.; Cramer, R. D.; Jones, D. M.; Patterson, D. E.; Simeroth, P. E. *Tetrahedron Comp. Methods* **1990**, *3*, 47.
16. *3D-QSAR in Drug Design. Theory, Methods and Applications*. Kubinyi, H., Ed. ESCOM: Leiden, Netherlands, 1993.
17. Klebe, G.; Abraham, U.; Mietzner, T. *J. Med. Chem*. **1994**, *37*, 4130.
18. Baroni, M.; Costantino, G.; Cruciani, G.; Riganelli, D.; Valigi, R.; Clementi, S. *Quant. Struct.-Act. Relat*. **1993**, *12*, 9.
19. Matter, H.; Schwab, W.; Barbier, D.; Billen, G.; Haase, B.; Neises, B.; Schudok, M.; Thorwart, W.; Schreuder, H.; Brachvogel, V.; Lönze, P.; Weithmann, K.-U. *J. Med. Chem*. **1999**, *42*, 1908.
20. Matter, H.; Schwab, W. *J. Med. Chem*. **1999**, *42*, 4506.
21. Residue numbering follows pro HNC nomenclature Hasty, K. A.; Pourmotabbed, T. F.; Goldberg, G. I.; Thompson, J. P.; Spinella, D. G.; Stevens, R. M.; Mainardi, C. L. *J. Biol. Chem*. **1990**, *265*, 11421.
22. Goodford, P. J. *J. Med. Chem*. **1985**, *28*, 849.
23. Hodgson, J. *Bio/Technology* **1995**, *13*, 554.
24. Chapman, K. T.; Durette, P. L.; Caldwell, C. G.; Sperow, K. M.; Niedzwiecki, L. M.; Harrison, R. K.; Saphos, C.; Christen, A. J.; Olszewski, J. M.; Moore, V. L.; Maccoss, M.; Hagmann, W. K. *Bioorg. Med. Chem. Lett*. **1996**, *6*, 803.
25. (a) Caldwell, C. G.; Sahoo, S. P.; Polo, S. A.; Eversole, R. R.; Lanza, T. J.; Mills, S. G.; Niedzwiecki, L. M.; Izquierdo-Martin, M.; Chang, B. C.; Harrison, R. K.; Kuo, D. W.; Lin, T. Y.; Stein, R. L.; Durette, P. L.; Hagmann, W. K. *Bioorg. Med. Chem. Lett*. **1996**, *6*, 323. (b) Chapman, K. T.; Wales, J.; Sahoo, S. P.; Niedzwiecki, L. M.; Izquierdo-Martin, M.; Chang, B. C.; Harrison, R. K.; Stein, R. L.; Hagmann, W. K. *Bioorg. Med. Chem. Lett*. **1996**, *6*, 329. (c) Beeley, N. R. A.; Ansell, P. R. J.; Docherty, A. J. P. *Curr. Opin. Ther. Pat*. **1994**, *4*, 7.

26. Levy, D. A.; Lapierre, F.; Liang, W.; Ye, W.; Lange, C. W.; Li, X.; Grobelny, D.; Casabonne, M.; Tyrrell, D.; Holme, K.; Nadzan, A.; Galardy, R. E. *J. Med. Chem.* **1998**, *41*, 199.
27. Burley, S. K.; Petsko, G. A. *Science* **1985**, *229*, 23.
28. (a) Jones, G.; Willett, P.; Glen, R. C. *J. Comp.-Aided Mol. Des* **1995**, *9*, 532. (b) Implemented in: *SYBYL Molecular Modelling Package*, Version 6.4; Tripos: St. Louis, MO, USA, 1997.
29. Thorwart, W.; Schwab, W.; Schudok, M.; Haase, B.; Bartnik, E.; Weithmann, K. U. *Ger. Offen* CODEN: GWXXBX. DE 19542189 A1 970515. CAN 127:50547.
30. (a) Cox, E. D.; Cook, J. M. *Chem. Rev.* **1995**, *95*, 1797. (b) Lorsbach, B. A.; Kurth, M. J. *Chem. Rev.* **1999**, *99*, 1549.
31. Schudok, M. European Patent Application 0878467.
32. Gavuzzo, E.; Pochetti, G.; Mazza, F.; Gallina, C.; Gorini, B.; D'Alessio, S.; Pieper, M.; Tschesche, H.; Tucker, P. A. *J. Med. Chem.* **2000**, *43*, 3377.
33. Biological activities are expressed in general as $\log(1/IC_{50}* 100{,}000)$.
34. Artursson, P.; Palm, K.; Luthman, K. *Adv. Drug Deliv. Rev.* **2001**, *46*, 27.
35. Caldwell, G. W. *Curr. Opin. Drug Discov. Dev.* **2000**, *3*, 30.
36. t1/2β: terminal halflife; CMC: Carboxymethylcellulose; DONSS: Dioctylsulfosuccinate; Fluka 86139.
37. Begtrup, M.; Holm, J. *J. Chem. Soc., Perkin Trans. 2* **1981**, 503.
38. Weithmann, K. U.; Schlotte, V.; Jeske, V.; Seiffge, D.; Laber, A.; Haase, B.; Schleyerbach, R. *Inflamm. Res.* **1997**, *46*, 246.
39. Knight, C. G.; Willenbrock, F.; Murphy, G. *FEBS Lett.* **1992**, *296*, 263.
40. *SYBYL Molecular Modeling Package*, Versions 6.3, 6.4 and 6.5; Tripos: St. Louis, MO, USA, 1996–1998.
41. Clark, M.; Cramer, R. D.; Van Opdenbosch, N. *J. Comp. Chem.* **1989**, *10*, 982.
42. Gasteiger, J.; Marsili, M. *Tetrahedron* **1980**, *36*, 3219.